Eur. Phys. J. B **4**, 499–511 (1998)

THE EUROPEAN PHYSICAL JOURNAL B

On some natural and model 2D bimodal random cellular structures

V. Parfait-Pignol[1], G. Le Caër[2,a], and R. Delannay[1,b]

[1] Laboratoire d'Énergétique et de Mécanique Théorique et Appliquée[c], École des Mines, Parc de Saurupt, 54042 Nancy Cedex, France
[2] Laboratoire de Science et Génie des Matériaux Métalliques[d], École des Mines, Parc de Saurupt, 54042 Nancy Cedex, France

Received: 24 December 1997 / Revised: 7 April 1998 / Accepted: 20 April 1998

Abstract. The topological and metric properties of a few natural 2D random cellular structures, namely an armadillo shell structure and young soap froths, which are formed from two classes of cells, large and small, have been characterized. The topological properties of a model generated from a Kagome tiling, which mimics such random binary structures, have also been exactly calculated. The distribution of the number of cell sides is bimodal for the structures investigated. In contrast to the classical Aboav-Weaire law for homogeneous 2D random cellular structures, $nm(n)$, the mean total number of edges of neighbouring cells of cells with n sides does not vary linearly with n. Only the $nm(i,n)$ $(i=1,2)$ determined separately for every class of cells are linear in n for all investigated structures. Topological properties and correlations between metric and topological properties are finally compared with the predictions of various literature models.

PACS. 05.90.+m Other topics in statistical physics and thermodynamics – 82.70.Rr Aerosols and foams

1 Introduction

Two-dimensional (2D) space-filling random cellular structures occur frequently in nature. They divide space into cells which have generally a rather regular shape with at least three sides. In most random structures, there are three cells meeting at a vertex. Many studies (for instance on 2D soap froths [1–5], on planar sections of metallurgical aggregates [6,7], or on biological tissues [8–12]) have been devoted to the characterization of 2D cellular structures. The features most often investigated are:

- one-cell characteristics: the probability distribution $p(n)$ of the number n of edges of cells (a n-cell designates hereafter a cell with n edges) whose variance μ_2 conveniently characterizes the disorder of the structure, $\mu_2 = \langle n^2 \rangle - \langle n \rangle^2$, where $\langle n \rangle$ is equal to 6 for infinite structures. Usually, $p(n)$ distributions are unimodal,
- two-cell characteristics: the total average number $nm(n)$ of edges of cells adjacent to n-cells. It has been observed over the last twenty years that $nm(n)$ varies fairly linearly with n (Aboav-Weaire law [13–18]). Two-cell correlations which extend beyond the first neighbour shell have only recently been characterized experimentally in soap froths [5], theoretically or in computer generated models [19–21],
- metric characteristics: the average area $a(n)$ of n-cells. In most cases $a(n)$ is an increasing function of n (see for instance [8,9,12,18,21]), often linear (Lewis' law [8,9]).

Most 2D random structures previously investigated are homogeneous and are constructed from one family of cells. Characteristics of some heterogeneous 2D structures with two main families of cells have only been recently reported. Annic *et al.* [22] have performed detailed studies of random mosaics obtained by radical tessellations of packing of discs (RTD) (radical tessellations are also named Laguerre tessellations [23,24]) with two different sizes in statistical equilibrium on an air table [25]. For given proportions of small and large discs and low packing fraction, the distribution $p(n)$ has a usual unimodal behaviour. But at large enough packing fraction, it becomes bimodal. We define here a bimodal structure as a cellular structure whose cells can be unambiguously divided into two classes of cells using for instance an area criterion or an edge number criterion and which shows a bimodal area distribution or (and) a bimodal $p(n)$ distribution. The latter structures consist in two classes, class 1 and class 2, which contain the smaller and the larger cells respectively. The following

[a] e-mail: `lecaer@mines.u-nancy.fr`
[b] *Permanent address*: Groupe Matière Condensée et Matériaux, CNRS UMR C6626, Université de Rennes-I, avenue du Général Leclerc, 35042 Rennes Cedex, France.
[c] CNRS UMR 7563.
[d] CNRS UMR 7584.

notations are used for the characteristics of subpopulation i ($i = 1, 2$):

- $p_i(n)$ is the edge number distribution normalized to 1 for each i;
- $\langle n \rangle_i$ is the mean number of edges of cells which belong to class i:

$$\langle n \rangle_i = \sum_n n p_i(n); \tag{1}$$

- $(\mu_2)_i$ is the variance of the distribution $p_i(n)$:

$$(\mu_2)_i = \sum_n \big(n - \langle n \rangle_i\big)^2 p_i(n). \tag{2}$$

The edge number distribution $p(n)$ is written as:

$$p(n) = \alpha p_1(n) + (1 - \alpha) p_2(n) \tag{3}$$

where α is the proportion of small cells.

The RTD which is more specifically considered here has, by construction, $\alpha = 0.5$ with disc radii $R_1 = 0.5$ cm and $R_2 = 1$ cm and a packing fraction $C = 0.73$ [22]. The distributions of edge numbers and of areas are peaked around two values which clearly characterize the two size classes. Moreover the variations of $nm(n)$ and of $a(n)$ with n are no more linear but S-shaped. As shown by Annic *et al.* [22], the n dependence of $nm(n)$ can be accounted for by two linear parts each associated with one of the previous classes. These two straight lines seem to have the same slope but have two different intercepts. Rivier has used maximum entropy inference to explain these experimental results [26].

The aim of the present paper is to study some topological and metric properties of natural and model 2D bimodal random structures and to compare their characteristics with those of the previous RTD.

2 Bimodal structures

To obtain the metric and topological properties of the various structures, images were first recorded with a video CCD camera (Fig. 1). The images were then analyzed with the software VISILOG which yields the studied cellular structures in which all actual edges are replaced by straight lines.

The images were further analyzed with the help of the software package 2DCELL [28]. The vertices and edges of every cell which are totally included in the analyzed framework were then determined. The metric and topological properties of the latter cells were calculated. Some characteristics, for instance the pair correlation's $nm(n)$, were determined only for cells whose neighbourhood is totally known (an example of such a characterization can be found in [29]). Because of the sampling performed by the analysis window, larger cells have a larger probability to be cut by the framework than smaller cells. The results are therefore statistically biased. A bias correction, based on the Miles and Lantuejoul's method, was performed [4]. The differences between the corrected and raw edge number distributions are however negligible (Fig. 2b) and were not performed for the subpopulation characteristics.

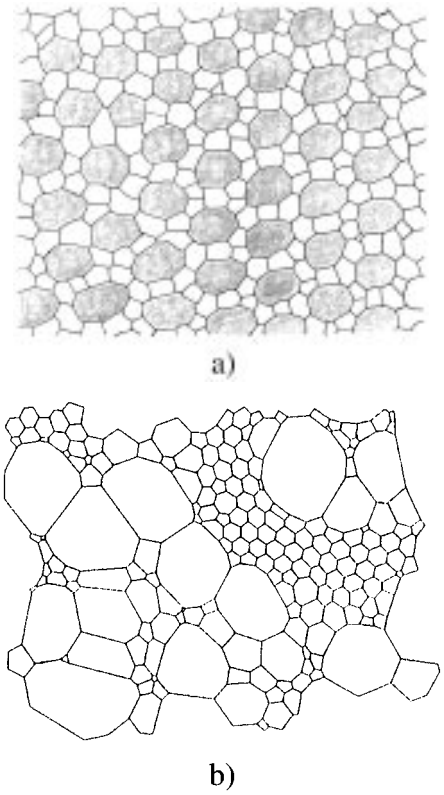

Fig. 1. a) Cell structure associated with the bony plates of an armadillo's shell (large cells which belong to subpopulation 2 are greyish). b) Young soap froth aged for 140 h.

2.1 Armadillo's shell structure

The armadillo is an animal which lives in South America. Its body, which is about 30 cm long, is covered by a shell which is composed of bony plates. The cellular structure of Figure 1a (shell structure) is obtained from a photograph of an armadillo's shell which shows large and bright scales (represented as grey cells in Fig. 1a) which are surrounded by small and dark scales [30]. The actual scale of the structure, which is missing on the original picture [30], is however not relevant here as only relative metric properties will be considered. It is difficult to have an idea of the actual curvature of the part of the shell shown by the picture. However, cell edges are clear and sharp as expected for a photograph which is in focus. The shell structure is further very regular as shown by cell sizes and cell shapes. Both facts suggest that the picture has been taken in a region of the shell which is not strongly curved. We have thus ignored the problem raised by the curvature of the shell and we have assumed that it is flat. The problem of random bimodal structures in 2D curved spaces would also be worth being considered.

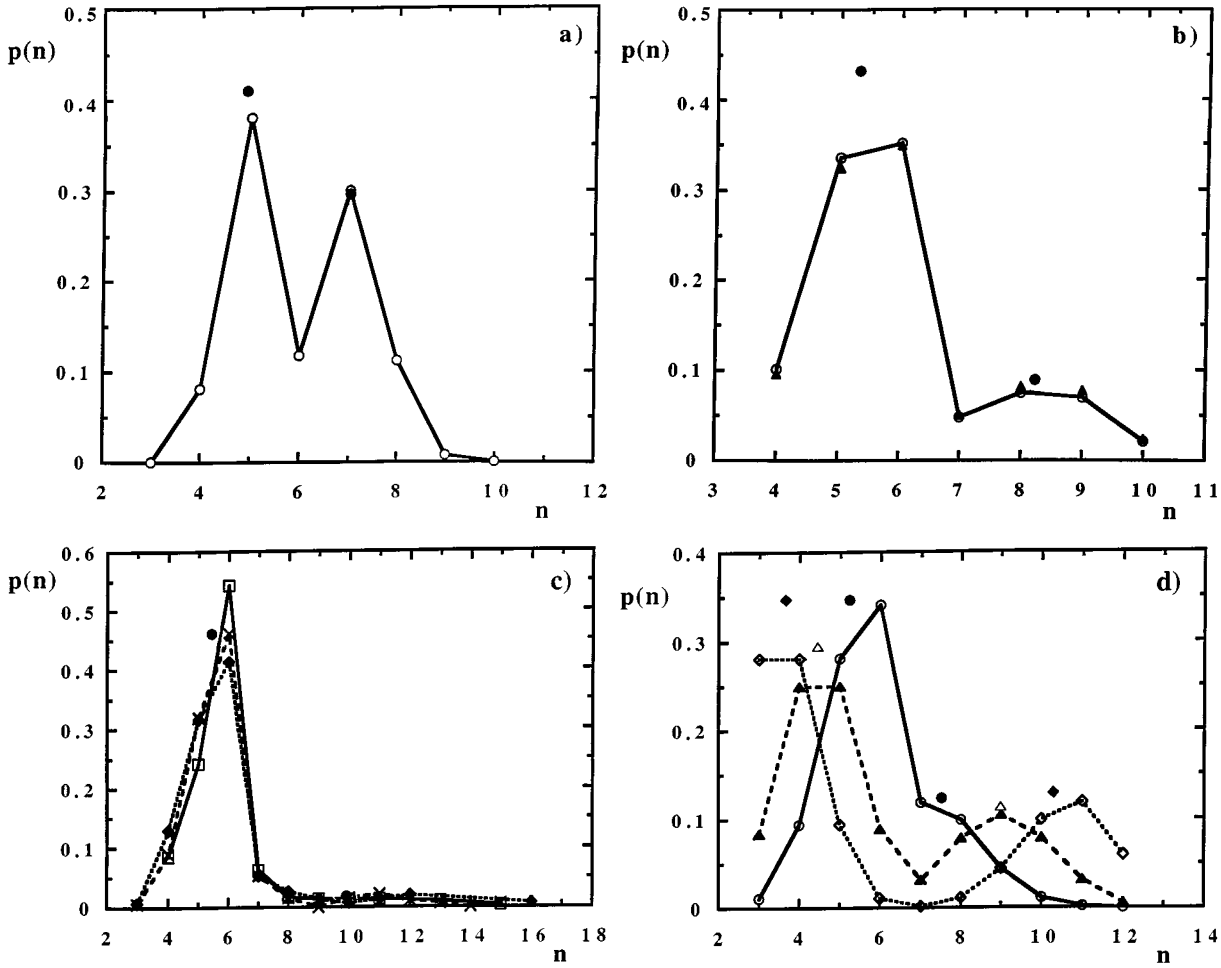

Fig. 2. Edge number distributions for: a) a RTD with $C = 0.73$ [22]; b) the shell structure (without bias correction: empty squares, with bias correction: full triangles); c) young soap froths aged for 110 h (empty squares), 140 h (crosses) and 152 h (full diamonds); d) Kagome structures with $p = 0.25$ (empty circles), 0.5 (full triangles), 0.75 (empty diamonds) respectively. In all cases, the values $\alpha p_1(\langle n \rangle_1)$ and $(1-\alpha)p_2(\langle n \rangle_2)$ are shown with the same symbols as those used for $p(n)$ but the symbols are empty when the latter are full and *vice-versa*.

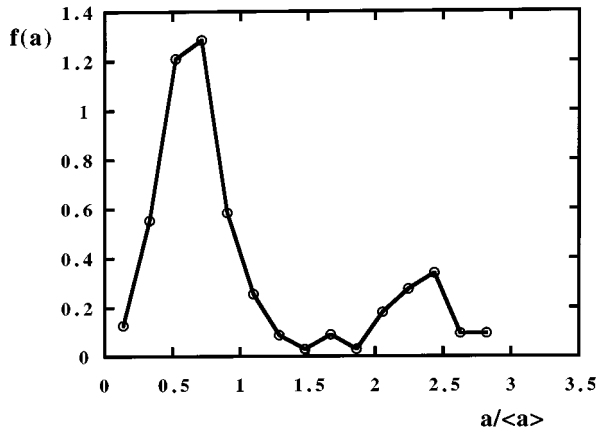

Fig. 3. Reduced area distribution for the shell structure.

Figures 2a, b show the edge number distributions reported for the RTD and for the shell structure respectively. The variance μ_2 and $p(6)$ are given in Table 1. The proportions of small cells are $\alpha = 0.5$ and $\alpha = 0.8$ respectively. For the shell structure, the distribution $p(n)$ is peaked around two values close to 5-6 for small cells, and close to 8-9 for large cells. Peak positions, which are typical of a given bimodal structure, depend on the types of cells. The bimodality of both structures is thus also clearly evidenced in terms of distribution of topological classes. Figure 3 further shows the bimodal distribution of reduced cell areas $a(n)$ (with an average cell area equal to 1) for the shell structure.

2.2 Topological model associated with a Kagome tiling

Simultaneous trends for cells with few sides to be surrounded by cells with many sides and for the average area of n-cells to increase monotonically with n (for instance Lewis's law and Desch's law) are observed to hold in natural structures. Small cells tend thus to have few sides while large cells tend to have many sides. It is thus quite natural, as already proposed [31], to investigate the

Table 1. Observed and calculated $p(6)$ values for various bimodal structures.

Structures	Topological disorder μ_2	$p(6)$	Value of $p(6)$ calculated from Eq. (4)
RTD ($C = 0.73$)	1.52	0.12	0.31
Shell	2.04	0.35	0.27
Kagome $p = 0.4$	3.84	0.159	0.195
Young soap froth (140 h)	2.65	0.46	0.24

Table 2. Edge number distribution $p(n)$ for Kagome cellular structures.

n	$p(n)$
3	$(2/3)p^3$
4	$2p^2(1-p)$
5	$2\ p(1-p)^2$
6	$(2/3)(1-p)^3 + (1/3)(1-p)^6$
7	$2(1-p)^5 p$
8	$5(1-p)^4 p^2$
9	$(20/3)(1-p)^3 p^3$
10	$5(1-p)^2 p^4$
11	$2(1-p)p^5$
12	$(1/3)p^6$

topological properties of models of bimodal space-filling random structures which are generated from regular patterns with two populations of polygons with less and more than six sides respectively. The initial pattern chosen here is the Kagome net, a two-dimensional structure constituted only of triangles and hexagons, in which four edges meet at every vertex (Fig. 4a). There are two triangles for one hexagon. As explained in previous papers [31,32], every vertex which belongs to more than three cells is topologically unstable in 2D structures. The construction method is based on removal of this instability. In the case of tetravalent vertices, the fourfold degeneracy of each vertex of the mother structure can be lifted at random as shown by Figure 4a. There is an edge which is added at random and independently at each vertex so that the hexagons gain an edge with a probability p. The final structure is by construction a structure with trivalent vertices, named here Kagome structure. The triangles of the mother Kagome net give rise to cells which may have from 3 to 6 edges and constitute class 1. The initial hexagons yield cells whose number of edges may vary from 6 to 12 edges. As explained previously, such many-sided cells constitute class 2. Possible realizations of bimodal cellular structures are shown in Figures 4b, c for two different values of p ($p = 0.25$ and $p = 0.75$).

Only topological properties can be calculated for such model structures. For a given mother structure, they depend only on the probability p defined earlier. As there are two triangles for each hexagon in the Kagome net, the proportion α is equal to $2/3$, whatever p. The distribution of the number of edges of cells is given in Table 2. The associated topological disorder is $\mu_2 = 2p(2+7p)$. Figure 2d shows distributions $p(n)$ obtained for three different values of p ($p = 0.25$, 0.5 and 0.75). The two peaks of $p(n)$ become closer as p decreases from 0.75 to 0.25. This is because the structure consists only of 3-cells and of 12-cells for $p = 1$ while it is built only from 6-cells for $p = 0$.

The topological characteristics, $\langle n\rangle_i$ and $(\mu_2)_i$ ($i = 1,\ 2$), are calculated from Bernoulli trials for every class:

- class 1 (generated from triangles): $\langle n\rangle_1 = 6 - 3p$, $(\mu_2)_1 = 3p(1-p)$,
- class 2 (generated from hexagons): $\langle n\rangle_2 = 6(1+p)$, $(\mu_2)_2 = 6p(1-p)$.

The pair correlation $nm(n)$, still defined as the total average number $nm(n)$ of edges of cells of both classes which are adjacent to n-cells, is bilinear in n and p as shown in Appendix A:

- for $n < 6$ (class 1): $nm(n) = 2(2-p)n + 6(1+3p)$
- for $n > 6$ (class 2): $nm(n) = 5(1+p)n + 6(1-6p)$.

As 6-cells are shared by both populations, $6m(6)$ is calculated from an average over the values of $6m(6)$ for classes 1 and 2 and for $p < 1$ (Appendix A):

$$6m(6) = 36 + \frac{6p\left(1 - \dfrac{(1-p)^3}{2}\right)}{1 + \dfrac{(1-p)^3}{2}}\,.$$

The slopes of the two lines, $nm(n)$ *versus* n with $n < 6$ and $n > 6$ respectively, are different whatever p as justified in detail in Appendix A. Other topological models of bimodal cellular structures might be constructed in a similar way from different mother structures. Appendix B describes for instance a model, with $\alpha = 8/9$, generated from a mother Archimedean tiling ($3^4.6$), constituted of triangles and hexagons, with pentavalent vertices (Fig. 11).

A different topological model of binary 2D random cellular structures, intended to account for properties of binary disc assemblies, has been recently proposed by Schliecker [33]. It performs restricted neighbour switching transformations (T_1) in tilings whose vertices are already trivalent. Exact calculations are performed for instance for a tiling made from a periodic arrangement of squares and octagons in which dynamical T_1 occur with a given probability p only on the edges shared by the octagons. The model incorporates thus two classes of cells

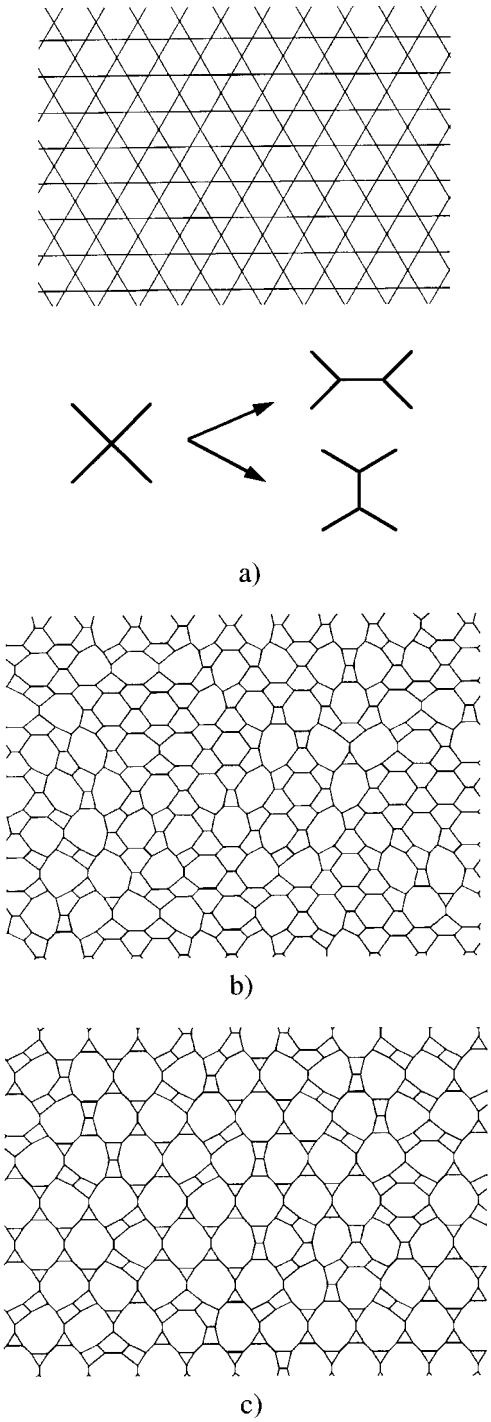

Fig. 4. Kagome structure: a) mother structure and the two stable transformations of a tetravalent vertex, b) and c) realizations of daughter structures for $p = 0.25$ and $p = 0.5$ respectively.

which originate from the two mother polygons. Equilibrium properties of the resulting structures depend on p. Like the structures considered here, they are characterized for most p values by bimodal edge number distributions and by correlations $nm(n)$ which are linear only for each class while the total correlation is not.

2.3 Young soap froths

We will also consider, although in less detail, two-dimensional soap froths formed between two glass plates, spaced by 2 or 3 mm [4]. They are prepared in the following way: the space between the two plates is first filled with a foaming liquid which is either some dishwashing liquid or sodium dodecyl sulphate (SDS) powder. Some glycerol is added to stabilize the foam. Bubbles are then produced by injecting air. When the air bubbles have nearly the same size, an initially ordered structure with almost only 6-cells is obtained. By contrast, an initially disordered foam structure, with cells of different sizes and numbers of edges, is formed when the injected air bubbles have different sizes.

The aging of initially ordered 2D soap froths take place in two steps, as described in [1,4]. The first transient stage consists of the propagation of topological disorder. It is followed by the scaling state regime where topological and scaled metric properties become stationary. In our experimental conditions, the latter regime is reached after aging for about 300 h.

We focus here on the characterization of the structures formed during the first transient step of the ordered soap froth's evolution whose cell repartitions with unmixed large and small cells differ from those of the RTD and of the armadillo's scale. Three structures aged for 110 h, 140 h and 152 h respectively have been investigated. During that transient step, disorder propagates and a structure with two types of zones, which do not mix, is progressively formed (Fig. 1b). One zone includes the small initial cells which are mostly six-sided. The other zone is formed from larger cells whose number of edges is in general larger than 6. The cells which belong to class 2 are taken here as those whose reduced area is larger than 1.5, a reasonable figure deduced from the n dependence of $a(n)$. The proportion α is large as compared to the aforementioned proportions, being for instance equal to 0.9 for an aging time of 140 h (see also Tab. 1). The edge number distribution (Fig. 2c) exhibits a second maximum with a reduced amplitude for $n = 11$. As the numbers of cells in subpopulation 2 is small, some young soap froth characteristics will be given mainly for information.

3 Results and discussion

3.1 Edge number distribution and topological disorder

A universal relation, which connects the variance μ_2 to $p(6)$, was observed to hold for disordered cellular structures with overall homogeneous cell sizes by Lemaître *et al.* [34]. Quantitative relations were proposed by Le Caër and Delannay [35] from a study of various $p(n)$ families:

$$\mu_2 p(6)^2 = 0.150\,(\pm 0.014) \quad 0.1 \leq p(6) \leq 0.7. \qquad (4)$$

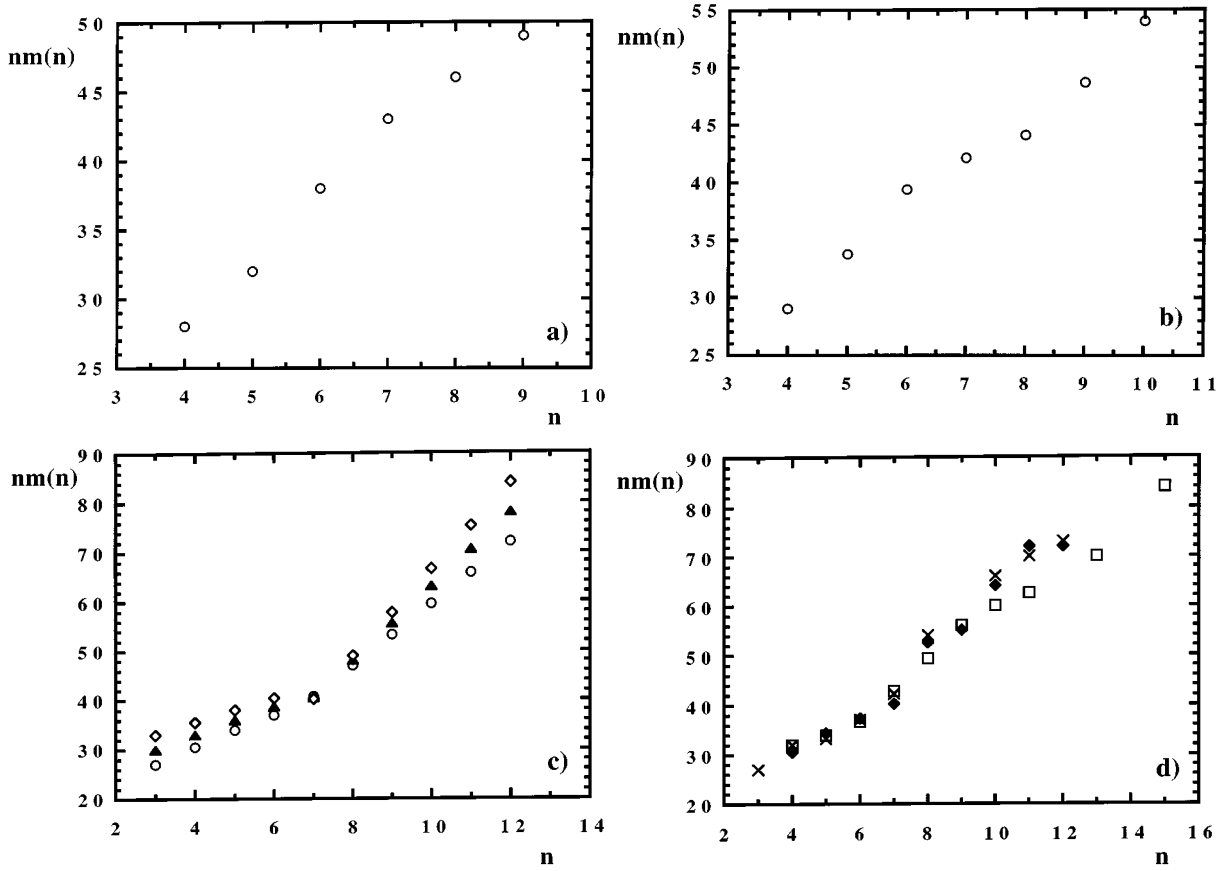

Fig. 5. Mean total number of sides $nm(n)$ of the first neighbour cells of n-sided cells for: a) a RTD with $C = 0.73$ [22]; b) the shell structure; c) three Kagome structures ($p = 0.25$ (empty circles), 0.5 (full triangles), 0.75 (empty diamonds)); d) young soap froth structures aged for 110 h (empty squares), 140 h (crosses) and 152 h (full diamonds).

For approximately the same range of $p(6)$, Rivier derived the following relation [27]:

$$\mu_2 p(6)^2 = \frac{1}{2\pi} = 0.159... \tag{5}$$

Using maximum entropy inference. The previous relations have a priori no reason to be verified for the binary structures considered here. Annic *et al.* [22] noticed indeed that it is not valid for the bimodal structures they investigated (Tab. 1, some RTD results communicated by Troadec have also been included). The same conclusion holds for the structures studied here (Tab. 1). If we consider the way relation (4) was derived [35] for various families of discrete probability distributions, we notice that it is verified for discrete, unimodal and smooth distributions $p(n)$ with n larger or equal to a minimum value n_m ($= 3$ in general) and whose average $\langle n \rangle$ (here 6) is only slightly larger than n_m. A similar relation would hold for distributions shifted by a certain amount k by simply replacing $p(6)$ by $p(6+k)$. It is thus tempting to test if equation (4) is still approximately valid for populations 1 and 2 separately with:

$$(\mu_2)_i p_i^2(\langle n \rangle_i) = 0.15 \tag{6}$$

for $0.1 \lesssim p_i\ (\langle n \rangle_i) \lesssim 0.7$. The values of $\langle n \rangle_i$, of $(\mu_2)_i$ and of $p_i\ (\langle n \rangle_i)$ (Eq. (6)) have been calculated for the investigated structures (Tab. 3). To avoid interpolating the $p(n)$ distributions, we just plot in Figures 2 and 12 the points $\big(\langle n \rangle_1,\ \alpha p_1(\langle n \rangle_1)\big)$ and $\big(\langle n \rangle_2,\ (1-\alpha) p_2(\langle n \rangle_2)\big)$. The relation proposed between $(\mu_2)_i$ and $p_i(\langle n \rangle_i)$ is seen to be reasonably obeyed and is expected to give useful indications about bimodal structures.

3.2 n dependence of nm(n)

The Aboav-Weaire law [13–15,17] is a semi-empirical law which relates linearly the total mean number $nm(n)$ of edges of the first neighbouring cells of n-cells to n:

$$nm(n) = (6 - a)n + 6a + \mu_2$$

where the Aboav-Weaire parameter a is of the order of 1 for natural unimodal structures. The n dependence of $nm(n)$ is neither linear for the bimodal RTD's nor for the present structures (Fig. 5). The linear behaviour holds however separately for the $nm(i,n)$ ($i = 1,\ 2$) of the two subpopulations. The pair correlation $nm(i,n)$ counts the average total number of sides of *all* cells which are first neighbours of n-cells belonging to class i. The n dependence of $nm(n)$ is S-shaped for the RTD [22] and for the young soap froth with a larger intercept for the $nm(2,n)$

Table 3. Observed values of $p_i([n]_i)$, where $[n]_i$ is the integer next lower or next higher than $\langle n\rangle_i$ (in some cases both are given), and calculated values of $p_i(\langle n\rangle_i)$ (Eq. (6)) for various bimodal structures.

Structures	$[n]_i$	Topological disorder $(\mu_2)_i$	$p_i([n]_i)$	Value of $p_i(\langle n\rangle_i)$ from Eq. (6)
RTD ($C = 0.73$) $\langle n\rangle_1 = 4.91$	5	0.23	0.76	0.82
RTD ($C = 0.73$) $\langle n\rangle_2 = 7.09$	7	0.44	0.60	0.59
Shell $\langle n\rangle_1 = 5.3$	5	0.53	0.45	0.54
Shell $\langle n\rangle_2 = 8.2$	8	0.74	0.44	0.45
Kagome $p = 0.3$ $\langle n\rangle_1 = 5.1$	5	0.63	0.441	0.488
$p = 0.3$ $\langle n\rangle_2 = 7.8$	8	1.26	0.324	0.345
Kagome $p = 0.4$ $\langle n\rangle_1 = 4.8$	5	0.72	0.432	0.456
$p = 0.4$ $\langle n\rangle_2 = 8.4$	8 9	1.44	0.311 0.276	0.323
Kagome $p = 0.5$ $\langle n\rangle_1 = 4.5$	4 5	0.75	0.375 0.375	0.44
$p = 0.5$ $\langle n\rangle_2 = 9$	9	1.5	0.3125	0.316
Kagome $p = 0.6$ $\langle n\rangle_1 = 4.2$	4	0.72	0.432	0.456
$p = 0.6$ $\langle n\rangle_2 = 9.6$	9 10	1.44	0.276 0.311	0.322
Kagome $p = 0.7$ $\langle n\rangle_1 = 3.9$	4	0.63	0.441	0.488
$p = 0.7$ $\langle n\rangle_2 = 10.2$	10	1.26	0.324	0.345
Kagome $p = 0.8$ $\langle n\rangle_1 = 3.6$	4 3	0.48	0.384 0.512	0.559
$p = 0.8$ $\langle n\rangle_2 = 10.8$	11	0.96	0.393	0.395
Young soap froth (140 h) $\langle n\rangle_1 = 5.5$	5 6	0.58	0.35 0.49	0.51
Young soap froth (140 h) $\langle n\rangle_2 = 9.9$	10	5.8	0.17	0.16

line than for the $nm(1,n)$ one while the reverse is observed for the shell structure. Maximum entropy inference applied by Rivier [26] to polydisperse froths predicts a linear dependence of $nm(i,n)$ on n (note Rivier used indices 2 and 1 for the subpopulations named here 1 and 2 respectively):

$$nm(n,1) = (6-a)(n-6) + X_1$$

$$nm(n,2) = (6-a)(n-6) + X_2$$

and the total $nm(n)$ is:

$$nm(n) = (6-a)(n-6) + q_{n1}X_1 + (1-q_{n1})X_2$$

with $q_{n1} = p_1(n)/(p_1(n)+p_2(n))$. Identical slopes, $6-a$, are thus expected for all lines in agreement with the RTD ($C = 0.73$) results ($a_1 = a_2 = 2$) [22]. Figure 6a shows that both $nm(i,n)$ vary also linearly with n for the shell structure. To compare the predictions of the previous model with experiment, we take for X_i ($i = 1,2$) the experimental values $6m(6,i)$, $X_1 = 39.5$ and $X_2 = 34$ respectively. The best fit to experiment is then obtained for

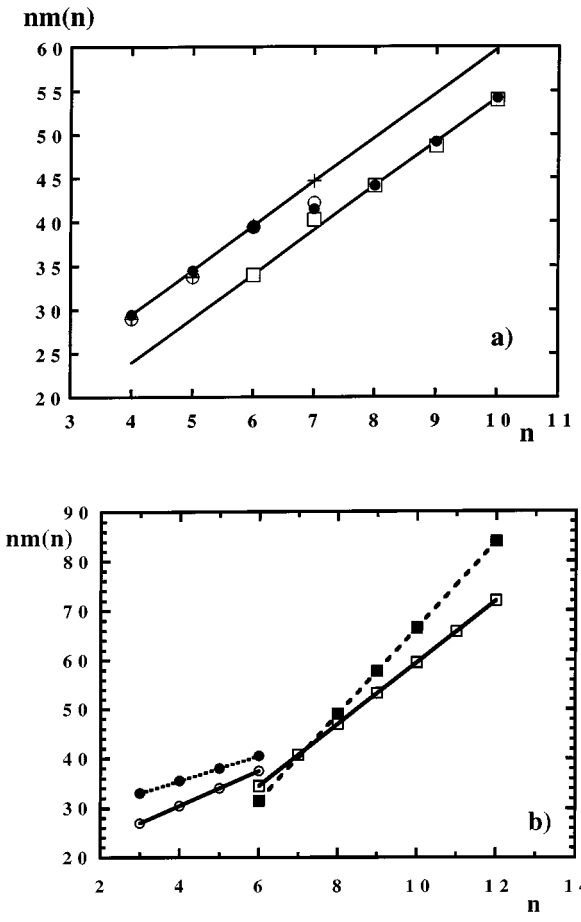

Fig. 6. Mean total number of sides $nm(n)$ for the two sub-populations of: a) the shell structure (crosses: $nm(1,n)$, empty squares: $nm(2,n)$, empty circles: experimental $nm(n)$): $nm(n)$ (solid circles) and the two solid lines were calculated from the Rivier model [26] (see text, Sect. 3.2); b) two Kagome structures with $p = 0.25$ (empty circles for class 1, empty squares for class 2) and $p = 0.75$ (full circles for class 1, full squares for class 2).

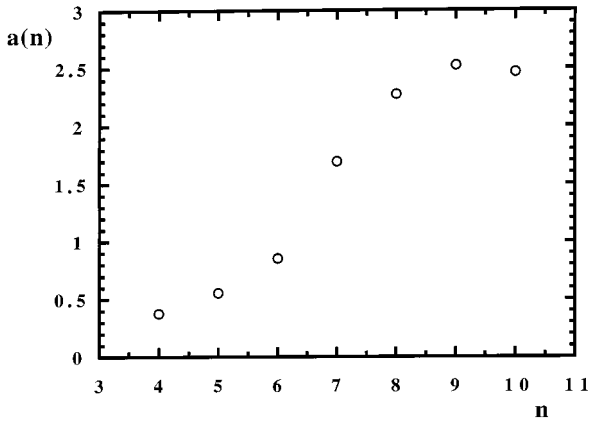

Fig. 7. Mean reduced area of n-sided cells $a(n)$ for the shell structure

$a = 0.95 \pm 0.05$. The latter method involves only three parameters. It is less sensitive to experimental errors than separate fits of each $nm(i,n)$ which require four parameters altogether. The Rivier model is seen to reproduce very well the experimental results (Fig. 6a). The relative values of X_1 and X_2 reflect the fact that large cells are exclusively surrounded by small cells [26]. The parameter $a = 0.95 \pm 0.05$ has a value similar to the typical value, $a \approx 1$, found for the Aboav-Weaire parameter in natural homogeneous structures.

For the Kagome structures (Sect. 2.2, Fig. 6b) and for the topological model of Schliecker [33], $nm(n)$ is still linear in n for every sub-population but the slopes of the two lines differ (Appendix A). For the Kagome structure, $7m(7) = 41 - p$ (Sect. 2.2 and Appendix A) depends only slightly on p as shown by Figure 5c. The overall shape of $nm(n)$ (Fig. 5c), in particular in the transition region between the two classes, is better understood from the relative positions and slopes of the lines associated with both topological classes (Fig. 6b). The Archimedean tiling $(3^6.4)$ generates a random structure whose $nm(n)$ bears some resemblance to the one of the shell structure (Appendix B, Figs. 11 and 13). The Schliecker model [33] is in statistical equilibrium but it would be associated with a binary packing of discs with a large size ratio R_2/R_1 not yet investigated experimentally. Such experiments would help to decide if an unique slope means almost surely that a given binary structure is in statistical equilibrium.

3.3 Correlations between metric and topological properties

The reduced areas of cells do not vary linearly (Lewis's law [8,9]) or quadratically (Desch's law) with the number of edges n in the shell structure (Fig. 7) or in the RTD (Fig. 5 of [22]). Similar S shapes are found for $a(n)$ in the both previous structures.

3.3.1 Correlations from models

Correlations between size and number of edges of cells have been worked out by various authors [36,37]. Some preliminary definitions are required to describe the published models:

- A, P area and perimeter of a cell respectively,
- equivalent circular radius, $R = \sqrt{A/\pi}$, which is the radius of a circular grain with area A,
- $\langle n \rangle_R$ mean number of edges of cells with a radius r: $R \leq r \leq R + dR$,
- $\langle R \rangle$ mean radius of cells.

The simplest relation has been named the "special linear relationship" (SLR) by Abbruzzese *et al.* [36]. This relation between size and number of cell sides was shown to have a wide range of validity, in particular in equiaxed

("quasi-circular") grain structures. The SLR [36] (Eq. (7)) is derived by assuming that the mean number $\langle n\rangle_R$ of edges of cells "with radius R", that is with $R - dR/2 \leq R \leq R+dR/2$, and the mean reduced radius $\langle r\rangle_n$ of n-cells depend linearly on R and on n respectively. Abbruzzese *et al.* [36] replace actual cells by discs and assume random surface covering for the probability of contacts between cells of different sizes. They obtain [36]:

$$\langle n\rangle_R = 3\left(1 + \frac{R}{\langle R\rangle}\right) \cdot \tag{7}$$

Thorvaldsen [37] has also derived relations between sizes and number of edges for 2D cells. In the stochastic field model [37], a particular cell of radius R is surrounded by cells whose size and accordingly number of sides vary randomly from neighbour to neighbour. The expected number of sides is inversely proportional to a contact angle he defines between two cells after having replaced them by discs. A factor ϕ ($\phi \leq 1$), independent of cell size, is introduced to correct for the latter approximation. The mean $\langle n\rangle_R$ depends explicitly on the distribution of R, on a circular aberration $P/(2\pi R)$ and on ϕ. The second model [37] is based on a mean field approximation in which the neighbours of a particular cell are replaced by cells of equal sizes. The mean-field relation is:

$$\langle n\rangle_R = \phi\pi + (6 - \phi\pi)\frac{R}{\langle R\rangle} \tag{8}$$

which reduces to the SLR for $\phi = 3/\pi \approx 0.955$.

The Dodds model [38–41] uses a completely triangulated ideal lattice to describe perfectly random polydisperse disc packings and to calculate coordination numbers among others. It may also be helpful to evidence deviations from a random repartition of two families of cells. If we assume, as done in the previous models, that every cell of class k ($k = 1, 2$) is replaced by a disc of radius R_k, the $\langle n\rangle_k$'s are calculated from:

$$\begin{aligned} x_k &= \beta_k\langle n\rangle_k/6 \\ &= (\beta_k\pi/3)/\left(x_k^2\pi/3 + x_1x_2(\pi - 2\theta_k) + 2\theta_{3-k}x_{3-k}^2\right) \end{aligned} \tag{9}$$

with $x_1 + x_2 = 1$, $\beta_1 = \alpha$, $\beta_2 = 1 - \alpha$,
and $\theta_k = \sin^{-1}\left(R_k/(R_1 + R_2)\right)$.

3.3.2 Comparison with experiment

Figure 8 shows the average numbers $\langle n\rangle_R$ of sides of cells of size ranging between $R - dR/2$ and $R + dR/2$ with $dR = 2.5$, 1.5 for the shell structure and the young soap froth respectively. Except for the mean-field model of Thorvaldsen (Eq. (8)), the comparisons between experiments and models are performed from experimentally determined parameters and not from fitted values. For the shell structure and for the young soap froth structures, R_k ($k = 1, 2$) is taken as the mean of the radii of cells belonging to subpopulation k.

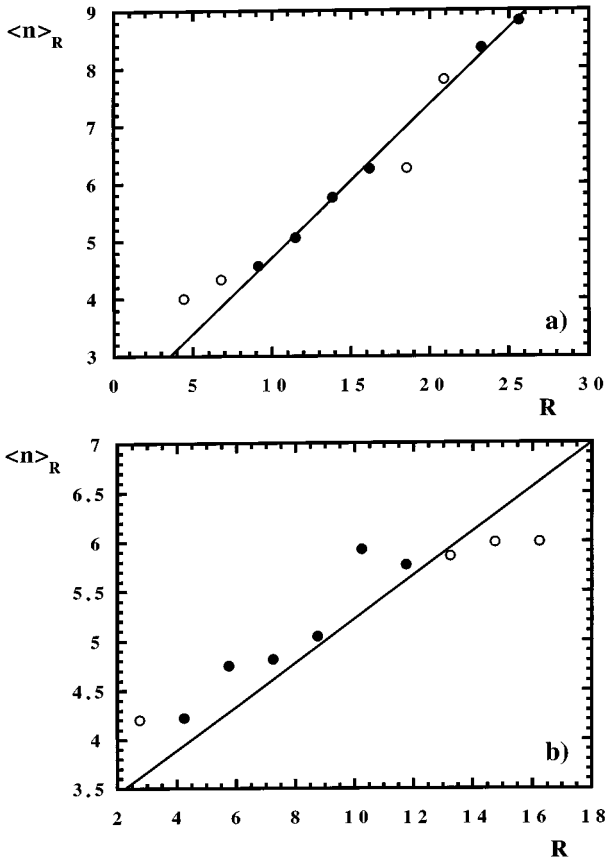

Fig. 8. Mean number of sides $\langle n\rangle_R$ of cells (empty circles: $\langle n\rangle_R$ calculated from less than ten cells, solid circles: $\langle n\rangle_R$ calculated from at least ten cells) for: a) the shell structure (solid line: linear fit obtained from solid circles) b) a young soap froth aged for 140 h (solid line: special linear relationship calculated from Eq. (7)).

a) For the RTD, with a packing fraction $C = 0.73$, the relevant parameters are $\alpha = 0.5$, $\langle n\rangle_1 = 4.91$ and $\langle n\rangle_2 = 7.09$, $R_2 = 2R_1$, $\langle R\rangle = (\alpha R_1 + (1 - \alpha)R_2) = R_1(2 - \alpha)$. Equation (7) gives $\langle n\rangle_1 = 5$ and $\langle n\rangle_2 = 7$ which agree well with experiment. It gives approximately the same results as those obtained for the considered tessellation from the general model developed by Troadec *et al.* (Fig. 3 in [42], or Figs. 6, 7 in [43]).

b) For the shell structure, $\alpha = 0.8$, $\langle n\rangle_1 = 5.33$, $\langle n\rangle_2 = 8.18$ and the average radii are $R_1 = 12.46$, $R_2 = 23.71$ (units in pixel), that is $\langle R\rangle = 14.71$.

The SLR (relation (7)) yields $\langle n\rangle_1 = 5.54$ and $\langle n\rangle_2 = 7.83$ when $R = R_1$, R_2 respectively. A least-squares linear fit of the $\langle n\rangle_R$ defined by at least ten cells gives however (Fig. 8a): $\langle n\rangle_R = 2.06 + 0.26R$, which differs from equation (7) ($\langle n\rangle_R = 3 + 0.204R$) and is consistent with relation (8) for $\phi = 0.67 \pm 0.02$. For the latter value of ϕ, relation (8) gives $\langle n\rangle_1 = 5.30$ and $\langle n\rangle_2 = 8.22$. For the Dodds model (Eq. (9)), we obtain $x_1 = 0.734$ and thus $\langle n\rangle_1 = 5.50$ and $\langle n\rangle_2 = 7.98$ which are close to the SLR values for R_1 and R_2. The fraction t_{km} of contacts between cells k and m ($k, m = 1, 2$) [39–41,44] is deduced to be: $t_{11} = 0.54$, $t_{12} = 0.39$, $t_{22} = 0.07$ in the Dodds model

while $t_{22} = 0$ is measured in the actual structure. The overall agreement with experiment is reasonable despite the simplifying assumptions done in the previous models and the replacement of every cell of a given class by a single disc. The repulsion effect is significantly evidenced in the Dodds model by the difference in the t_{22} values although it may appear to be small. Very large differences cannot be expected between an ordered repartition of two mixed species and a disordered one when the concentration of the minority species is rather low (it is here 20%).

c) For the young soap froth aged for 140 h, $\alpha = 0.9$, $R_1 = 10.155$, $R_2 = 38.48$ (units in pixel), $\langle R \rangle = 13$ and $\langle n \rangle_1 = 5.54$ and $\langle n \rangle_2 = 9.25$. The SLR (Eq. (7), Fig. 8b) gives $\langle n \rangle_1 = 5.34$ and $\langle n \rangle_2 = 11.88$. The Dodds model (Eq. (9)) yields $x_1 = 0.653$, that is $\langle n \rangle_1 = 4.35$, $\langle n \rangle_2 = 20.82$ and $t_{11} = 0.43$, $t_{12} = 0.45$, $t_{22} = 0.12$. Despite the statistical uncertainties on the $\langle n \rangle_2$ value, such differences between model and experiment are consistent with the fact that large and small cells are not randomly distributed but segregated as shown by Figure 1b.

4 Conclusion

The topological and metric properties of the natural and model 2D cellular structures made from two cell classes investigated in the present paper or previously reported [22] have similar characteristics. The distributions of the number of edges of cells is bimodal for the previous structures. In contrast to the classical Aboav-Weaire law for homogeneous 2D cellular structures with one family of cells, $nm(n)$, the mean total number of edges of neighbouring cells of cells with n sides does not vary linearly with n. Only the $nm(i, n)$ $(i = 1, 2)$ determined separately for every class of cells are linear in n for all the investigated structures. The slopes determined for the various classes are equal for the natural shell structure or for the RTD ($C = 0.73$) which is in statistical equilibrium on an air table. According to Rivier [26], such results are expected for structures in statistical equilibrium. In contrast, different slopes are found for the topological models investigated till now: Kagome structures and Schliecker model which is in equilibrium [33]. New experimental studies of binary structures are thus desirable to support the connection between equality of slopes and equilibrium more firmly. Similar S shapes are found for the n dependence of the cell areas in the shell and RTD structures. Correlations between metric and topological properties have further been compared with the predictions of various literature models, those of Abbruzzese *et al.* [36], of Thorvaldsen [37] and of Dodds [38], in which every cell is to a first approximation replaced by a disc. They give a reasonable agreement with experiment for the RTD ($C = 0.73$) and for the shell structure whose cell arrangement is more ordered than a random arrangement of discs with the same size ratio. Larger differences are found when the previous models are applied to the unmixed young soap froths.

We thank Prof. J.P. Troadec (Université de Rennes I) for communicating useful information about binary packings of discs.

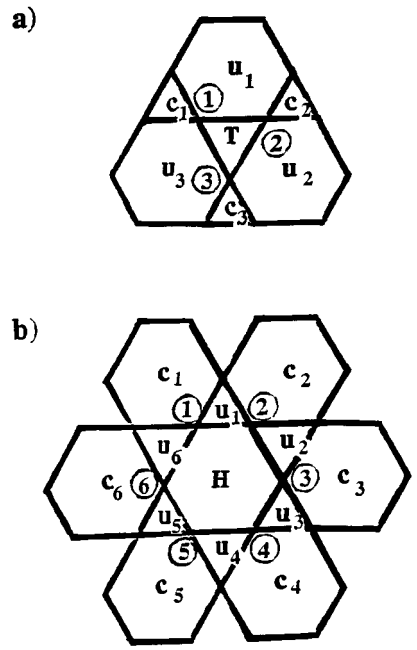

Fig. 9. A mother K-polygon ($K = T$, H), whose vertices are numbered from 1 to k (circled numbers), and its neighbours. The conditional neighbour c_j shares vertex number j with the central polygon. The unconditional neighbour u_j shares vertices j and $j + 1$ (*modulo* k) with it: a) the case of a central triangle; b) the case of a central hexagon.

Appendix A: Calculation of nm(n) for the Kagome structure

To simplify the description of the calculation of $nm(n)$, a K-polygon designates either a triangle ($K = T$) or a hexagon ($K = H$) of the Kagome net and k (=3 or 6) is its number of sides. Each K-polygon generates an n-sided K-cell in the final random structure ($3 \leq n \leq 6$ for $K = T$, $6 \leq n \leq 12$ for $K = H$). Classes 1 and 2 defined previously are named here T and H respectively. The vertices of the mother K-polygon are numbered from 1 to k (Fig. 9). We further define K_u as $K_u = H$ if $K = T$ and $K_u = T$ if $K = H$ and $k_u = k + 3(-1)^{k+1}$ as its number of sides. A "spin", $S = \pm 1/2$, is finally introduced [31] (Fig. 10). The spin allows description of the type of stable configuration which is chosen from the two possible at every mother lattice site (Fig. 4a). Figure 10 shows for instance the case of a 4-sided cell generated from a triangle. The spin value at a given vertex is taken as $+1/2$ when both hexagons gain one side once the instability is lifted at that vertex and $-1/2$ otherwise (Fig. 10). The value $+1/2$ is taken with a probability p, independently of the spin values at all other vertices (Bernoulli trials). The total number of edges of the n first neighbours cells of a given n-cell belonging to class K is defined as $nC_K(n)$ whose average over all n-cells of the same class yields $nm_K(n) = \langle nC_K(n) \rangle$.

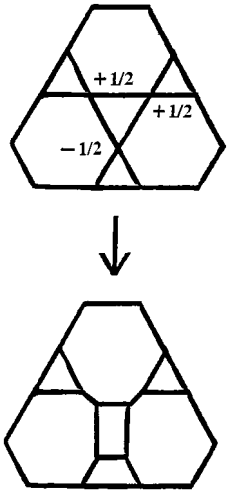

Fig. 10. A configuration of spins S at the vertices of a mother triangle and its daughter cell: a hexagon gains a side if $S = 1/2$, a triangle gains a side if $S = -1/2$.

As described in [31], n-cells generated from K-polygons of the Kagome net have two types of neighbours (Fig. 9):

1) k unconditional neighbours (u). They are associated with the k K_u-polygons which share one side with the central K-polygon. The unconditional neighbour u_j ($j = 1, ..., k$) shares vertices j and $j+1$ (*modulo* k) with the latter K-polygon.
2) $n-k$ conditional neighbours (c). Among the k K-polygons which share one vertex with the central K-polygon, only $(n-k)$ "active" K-polygons generate a neighbour of the central n-cell as their shared spin is equal to $(-1)^k/2$. The lowest triangle of Figure 10 generates for instance a neighbouring cell of the central cell as the shared spin is $-1/2$. The conditional neighbour c_j ($j = 1, ..., k$) shares vertex number j with the central K-polygon.
   As the contribution of vertex number j of a mother K-polygon to the total number of sides of the daughter K-cell is equal to $3/2+(-1)^k\, S_j$, the number n of sides of a K-cell is ($k = 3, 6$):

$$n = \frac{3k}{2} + (-1)^k \sum_{j=1}^{k} S_j. \tag{A.1}$$

To calculate $nC_K(n)$, the values of the k central spins (Fig. 9, S_j, $j = 1, ..., k$) are chosen so as to verify equation (A.1) and are then held fixed. Figure 9 shows all vertices needed for calculating $nC_K(n)$:

$$nC_K(n) = \sum_{j=1}^{k} \left\{ \sum_{i=1}^{ku} \left(\frac{3}{2} + (-1)^{ku} S_{uj}(i) \right) \right\} + \sum_{j=1}^{k} \left(\frac{1}{2} + (-1)^k S_j \right) \left\{ \sum_{j=1}^{k} \left(\frac{3}{2} + (-1)^k S_{cj}(i) \right) \right\}. \tag{A.2}$$

The first sum in equation (A.2) represents the contribution of unconditional neighbours: $S_{uj}(i)$ is the spin at the ith vertex of the unconditional neighbour u_j. Two among the latter k_u spins are S_j and S_{j+1} ($j+1$ *modulo* k) respectively (Fig. 9). The second sum represents the contribution of conditional neighbours. The factor $f_j = \big(1/2 + (-1)^k S_j\big)$ ($f_j = 1$ if $S_j = (-1)^k/2$ and $f_j = 0$ otherwise) ensures that only active neighbours contribute to the latter sum. $S_{cj}(i)$ is the spin at the ith vertex of the conditional neighbour c_j. One spin among the latter is S_j (Fig. 9). The average of $nC_K(n)$ for the given configuration of central spins is obtained by replacing, in equation (A.2), every outer spin by its average $\langle S \rangle = p - 1/2$ and by using equation (A.1). The resulting average depends only on n and p and is therefore equal to $nm_K(n)$. The various contributions to $nm_K(n)$ are thus:

a) unconditional neighbours (the terms in n are independent of p):

$$2(9/2 - n) + 12p + 21 \quad \text{for } K = T \tag{A.3}$$
$$2(9 - n) - 6p + 30 \quad \text{for } K = H \tag{A.4}$$

b) conditional neighbours (the terms in n depend on p):

$$(n - 9/2)(6 - 2p) - 3p + 9 \quad \text{for } K = T \tag{A.5}$$
$$(n - 9)(5p + 7) + 15p + 21 \quad \text{for } K = H \tag{A.6}$$

that is:

$$3 \le n \le 6: \quad nm_T(n) = 2(2-p)n + 6(2+3p) \tag{A.7}$$
$$6 \le n \le 12: \quad nm_H(n) = 5(1+p)n + 6(1-6p). \tag{A.8}$$

The probabilities of finding 6-sided K-cells are $p_T(6) = 2(1-p)^3/3$ and $p_H(6) = (1-p)^6/3$ for $K = T$, H respectively (Tab. 2). The average $6m(6)$ is thus:

$$6m(6) = 6\big(p_T(6)m_T(6) + p_H(6)m_H(6)\big)/\big(p_T(6) + p_H(6)\big). \tag{A.9}$$

Finally:

$$nm(n) = 2(2-p)n + 6(2+3p) \quad \text{for } 3 \le n \le 5$$

$$6m(6) = 36 + \frac{6p\left(1 - \dfrac{(1-p)^3}{2}\right)}{1 + \dfrac{(1-p)^3}{2}} \quad \text{for } n = 6 \text{ and } p < 1$$

$$nm(n) = 5(1+p)n + 6(1-6p) \quad \text{for } 7 \le n \le 12.$$

The slope of the line, $nm(n)$ *versus* n, is smaller for class T, $n < 6$, than it is for class H, $n > 6$. The contributions of both u and c neighbours to the total $nm(n)$ (Eqs. (A.3–A.6)) prove that the slope difference comes solely from conditional neighbours. The increase of the number

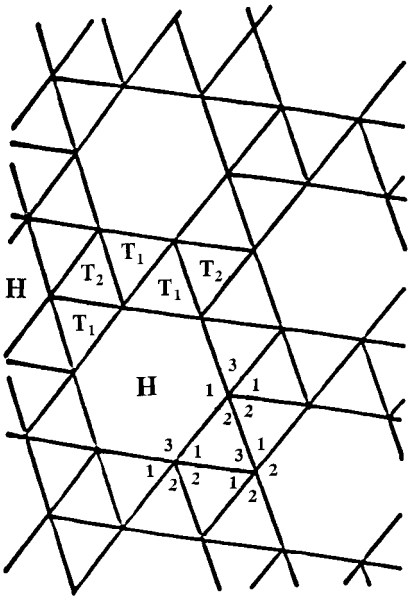

Fig. 11. Part of an Archimedean tiling ($3^6.4$) [44] formed from triangles T_1 and T_2 and from hexagons H. Examples of states [13122] ([32,35]) distributed on some vertices of the mother structure are also shown. A six-sided cell (1+2+3) will be generated from the lower left T_1 triangle with three integers inside.

of sides of a cell of a given class is indeed equal to the increase of the number of active conditional neighbours of its mother polygon. The increase with n of $nm(n)$ for cells generated from triangles is thus moderate as each active conditional neighbour of a triangle is a triangle (Fig. 9a). It generates cells with at most six sides. When a triangle becomes active, it gains a side which is the one shared with the central cell. It gains further an extra side with a probability $1-p$ at each of the two other vertices. A conditional neighbour has thus on the average $4+2(1-p) = 6-2p$ sides which is the n factor in equation (A.5). By contrast, each active conditional neighbour of a hexagon is a hexagon (Fig. 9b) which generates a cell with at least seven sides. Each active hexagon gains indeed a side shared with the central cell and gains an extra side with a probability p at each of the five other vertices. The average number of sides is thus $5p + 7$ which agrees with the term in n in equation (A.6).

The average $\langle nm(n)\rangle$, calculated from equations (A.7, A.8, A.9), is:

$$\langle nm(n)\rangle = \sum_{n=3}^{6} nm_T(n)p_T(n) + \sum_{n=6}^{12} nm_H(n)p_H(n)$$

that is: $\langle nm(n)\rangle = (2/3)[2(2-p)\langle n\rangle_T + 12 + 18p] + (1/3)[5(1+p)\langle n\rangle_H + 6(1-6p)]$. With $\langle n\rangle_T = 3(3/2 - \langle S\rangle) = 6 - 3p$, $\langle n\rangle_H = 6(3/2 + \langle S\rangle) = 6(1+p)$ and $\mu_2 = \langle (n-6)^2\rangle = 2p(2+7p)$ (see Sect. 2.2), we obtain finally: $\langle nm(n)\rangle = \mu_2 + 36 = \langle n^2\rangle$, as expected from the Weaire sum rule.

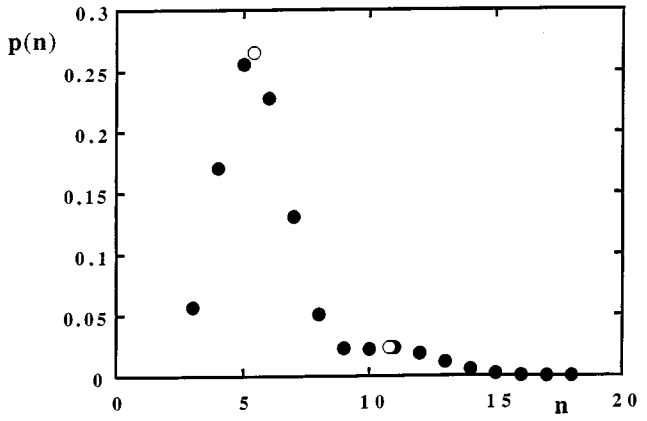

Fig. 12. Edge number distribution $p(n)$ (full circles) calculated for the T^4H structure. The values $\alpha p_T(\langle n\rangle_T)$ and $(1-\alpha)p_H(\langle n\rangle_H)$ ($\alpha = 8/9$) calculated from equation (6) are also shown (empty circles).

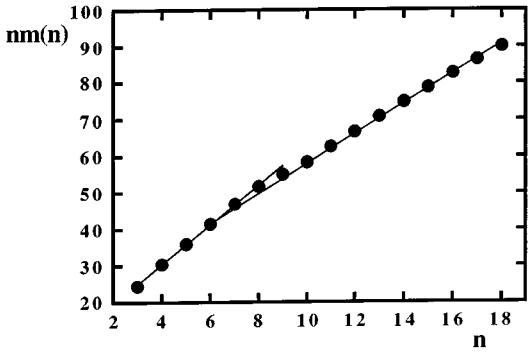

Fig. 13. Mean total number of sides $nm(n)$ (full circles) calculated for the T^4H structure. The solid lines are obtained from least-squares linear fits of $nm_T(n)$ ($3 \le n \le 9$) and of $nm_H(n)$ ($9 \le n \le 18$).

Appendix B: A 2D bimodal random structure generated from a ($3^4.6$) Archimedean tiling

There exist 11 distinct edge-to-edge tilings by regular polygons such that all vertices are of the same type [44]. Among the latter, the Archimedean tiling ($3^4.6$) by equilateral triangles and regular hexagons (Fig. 11), in which five edges meet at every vertex, occurs in two mirror image forms. Both enantiomorphic forms generate a unique 2D random structure when the degeneracy is lifted in the same way at every vertex. The mother tiling consist of hexagons H and of triangles T (Fig. 11). The class of triangles includes two types of triangles, T_1 and T_2, which have different neighbourhoods ((u) = unconditional, (c) = conditional (Appendix A)):

- triangles T_1: $H(u)$, $T_1(u)$, $T_2(u)$, $H(c)$, $2T_1(c)$; triangles T_2: $3T_1$ (u), $3H(c)$. Both classes of triangles T_1 and T_2 generate cells with $3 \le n \le 9$. Their respective weights are $\alpha_1 = 6/9$ and $\alpha_2 = 2/9$ ($\alpha = \alpha_1 + \alpha_2 = 8/9$)
- hexagons (H): $6T_1(u)$, $6T_1(c)$, $6T_2(c)$.

They generate cells with $6 \leq n \leq 18$ which represent 1/9 of all cells. As hexagons have no hexagon neighbours, many-sided cells of the daughter random structures have mostly few-sided cells as first neighbours.

The stable configuration is obtained by adding 2 sides at every pentavalent vertex [32,35]. There are thus 5 possible stable configurations called states [32]. Every state is characterized by a 5-dimensional vector $\mathbf{S}_i$ $(i = 1, .., 5)$. The five vectors $\mathbf{S}_i$ are (13122) and the four vectors obtained from it by circular permutations of its components. The sum of state components inside each polygon of the mother tiling is the number of sides of its daughter cell in the final random structure [32,35] (Fig. 11). The calculations of $p(n)$, of $nm_{T_1}(n)$, $nm_{T_2}(n)$ $(3 \leq n \leq 9)$ and of $nm_H(n)$ $(9 \leq n \leq 18)$ have been performed numerically for the sole case of equiprobable states as many particular configurations must be considered at the vertices of the various mother polygons. The state components at every vertex of the mother polygons are equal to 1, 2 and 3 with respective probabilities of 2/5, 2/5 and 1/5. We calculate as expected: $\langle n \rangle = 6$ and $\langle nm(n) \rangle = 40.7466667 \approx \langle n^2 \rangle = 3056/75$ for the daughter random cellular structure (T^4H structure). The distribution $p(n)$ is shown in Figure 12 ($\mu_2 = 356/75 \approx 4.7467$ and, $i = 1, 2$, $\langle n \rangle_{T_i} = \langle n \rangle_T = 5.4$, $\mu_{2T_i} = \mu_2 T = 1.68$, $\langle n \rangle_H = 10.8$, $\mu_{2H} = 3.36$). The n dependences of $nm_T(n)$ calculated from $nm_{T_1}(n)$ and $nm_{T_2}(n)$ and of $nm_H(n)$ are fairly (but not strictly) linear (Fig. 13). Disregarding the shift of the transition region towards larger values of n, we observe that the total $nm(n)$ (Fig. 13) resembles that of the shell structure (Fig. 6a). The branches of the inverted S are however not parallel as the slope of $nm_T(n)$ (5.45) is larger than the slope of $nm_H(n)$ (4.10).

References

1. J.A. Glazier, S.P. Gross, J. Stavans, Phys. Rev. A. **36**, 306 (1987).
2. J. Stavans, J.A. Glazier, Phys. Rev. Lett. **62**, 1318 (1989).
3. J. Stavans, Phys. Rev. A. **42**, 5049 (1990).
4. V. Pignol, *Évolution et caractérisation de structures cellulaires bidimensionnelles expérimentales, en particulier les mousses de savon, et simulées*, Ph.D. thesis, INPL Nancy, 1996.
5. K.Y. Szeto, T. Aste, W.Y. Tam, submitted (1997).
6. H.V. Atkinson, Acta Metall. **36**, 469 (1988).
7. V.E. Fradkov, D.G. Udler, Adv. Phys. **43**, 739 (1994).
8. F.T. Lewis, Anatom. Rec. **38**, 341 (1928).
9. N. Rivier, A. Lissowski, J. Phys. A: Math. Gen. **15**, L143 (1982).
10. N. Rivier, X. Arcenegui-Siemens, G. Schliecker, *Fragmentation Phenomena*, edited by D. Beysens, X. Campi, E. Perfferkorn, (World Scientific, Singapore, 1995), p. 266.
11. N. Rivier, B. Dubertret, Philos. Mag. B **72**, 311 (1995).
12. J.C.M. Mombach, R.M.C. De Almeida, J.R. Iglesias, Phys. Rev. E **47**, 3712 (1993).
13. D.A. Aboav, Metallography **3**, 383 (1970).
14. D. Weaire, Metallography **7**, 157 (1974).
15. D.A. Aboav, Metallography **13**, 43 (1980).
16. M.A. Fortes, J. Phys. A: Math. Gen. **28**, 1055 (1995).
17. M.A. Peshkin, K.J. Strandburg, N. Rivier, Phys. Rev. Lett. **7**, 1803 (1991).
18. D. Weaire, N. Rivier, Contemp. Phys. **25**, 59 (1984).
19. T. Aste, K.Y. Szeto, W.Y. Tam, Phys. Rev. E **54**, 5482 (1996).
20. B. Dubertret, N. Rivier, M.A. Peshkin, J. Phys. A: Math. Gen. **31**, 879 (1998).
21. K.Y. Szeto, W.Y. Tam, Physica A **221**, 256 (1995).
22. C. Annic, J.P. Troadec, A. Gervois, J. Lemaître, M. Ammi, L. Oger, J. Phys. I France **4**, 115 (1994).
23. H. Telley, T. Liebling, A. Mocellin, Philos. Mag. B **73**, 395 (1996).
24. H. Telley, T. Liebling, A. Mocellin, Philos. Mag. B **73**, 409 (1996).
25. J. Lemaître, A. Gervois, H. Peerhossaini, D. Bideau, J.P. Troadec, J. Phys. D: Appl. Phys. **23**, 1396 (1990).
26. N. Rivier, J. Phys. I France **4**, 127 (1994).
27. N. Rivier, *Statistical Mechanics to Statistical Inference and Back*, edited by Nadal, Grassberger (Kluwer, Dordrecht, 1994), p. 77.
28. F. Righetti, H. Telley, T.M. Liebling, A. Mocellin, Computer Phys. Comm. **67**, 509 (1992).
29. V. Pignol, R. Delannay, G. Le Caër, Acta Stereol. **12/2**, 149 (1993).
30. P.S. Stevens, *Les formes dans la nature* (Seuil, Paris,1978) Ch. 7, p. 179, Figure 152.
31. G. Le Caër, J. Phys. A: Math. Gen. **24**, 1307 (1991).
32. G. Le Caër, J. Phys. A: Math. Gen. **24**, 4655 (1991).
33. G. Schliecker, Phys. Rev. E **57**, R1219 (1998).
34. J. Lemaître, A. Gervois, D. Bideau, J.P. Troadec, M. Ammi, C. R. Acad. Sci. Paris Série II **315**, 35 (1992).
35. G. Le Caër, R. Delannay, J. Phys. A: Math. Gen. **26**, 3931 (1993).
36. G. Abbruzzese, I. Heckelmann, K. Lücke, Acta Metall. Mater. **40**, 519 (1992).
37. A. Thorvaldsen, J. Appl. Phys. **73**, 7831 (1993).
38. J.A. Dodds, Nature **256**, 187 (1975).
39. J.A. Dodds, *Physics of Granular Media*, edited by D. Bideau, J. Dodds (Nova Science Publishers, 1991), p. 57.
40. A. Gervois, D. Bideau, *Disorder and Granular Media*, edited by D. Bideau, A. Hansen (North Holland, Amsterdam, 1993), p. 57
41. J.P. Troadec, J.A. Dodds, *Disorder and Granular Media*, edited by D. Bideau, A. Hansen (North Holland, Amsterdam, 1993), p. 133
42. J.P. Troadec, A. Gervois, C. Annic, J. Lemaître, J. Phys. I, France **4**, 1121 (1994).
43. C. Annic, *Milieux Granulaires Modèles 2D: Distribution de taille, Ségrégation*, Ph.D. thesis, Université de Rennes I, 1994.
44. B. Grünbaum, G.C. Shephard, *Tilings and Patterns* (W.H. Freeman, New York, 1987), p. 63.